Journal of the Korean Society for Nondestructive Testing
Vol. 23, No. 6 (2003. 12)

Defect Shape Recovering by Parameter Estimation Arising in Eddy Current Testing

Fumio Kojima

Abstract This paper is concerned with a computational method for recovering a crack shape of steam generator tubes of nuclear plants. Problems on the shape identification are discussed arising in the characterization of a structural defect in a conductor using data of eddy current inspection. A surface defect on the generator tube can be detected as a probe impedance trajectory by scanning a pancake type coil. First, a mathematical model of the inspection process is derived from the Maxwell's equation. Second, the input and output relation is given by the approximate model by virtue of the hybrid use of the finite element and boundary element method. In that model, the crack shape is characterized by the unknown coefficients of the B-spline function which approximates the crack shape geometry. Finally, a parameter estimation technique is proposed for recovering the crack shape using data from the probe coil. The computational experiments were successfully tested with the laboratory data.

Keywords: Identification, inverse problems, parameter estimation, finite element method, boundary element method

1. Introduction

Quantitative nondestructive evaluation (QNDE) on steam generator (SG) tubes is a critical issue for the structural integrity of the pressurized water reactor nuclear plants (Takagi et al, 1994, 1995, 1996). The detection of a crack is not only to find out flaws but also to determine the size, shape, and orientation of each detective flaw. Eddy current testing (ECT) is used for in-service inspection of SG tubes because of high detectability and rapid scanning process. Although there exists wide range of tube degradation mechanisms, it is important to detect the surface crack inside and/or outside tubes. In this paper, a computational method is considered for estimating crack shape in conducting materials using data of eddy current inspections. Figure 1 shows the overall configuration of the inspection process. In this figure, a pancake type probe coil is used for the inspection of the tubes and defects can be detected as a probe impedance trajectory by scanning the probe coil. The inversion techniques using eddy current data have been studied computationally and experimentally by many authors (e.g., Sabbagh, 1986, Bowler et al, 1991, 1995, and Harrison et al, 1996, etc). Most efforts on inverse analyses have been directed to an identification of inhomogeneity of electrical conductivity by measuring impedance trajectories of the coil. In our approach, the recovery of crack shape can be formulated as a domain identification problem. Domain identification problems have been concentrated on the design of engineering systems which involve numerous applications to engine, airplane, etc (See Pironneau, 1983 and the references therein). Although the problem treated here is motivated by an application that is different from those shape design problems, the resulting computational aspects are closely related.

Received: September 8, 2003. Accepted: October 16, 2003. * Graduate School of Science and Technology, Kobe University 1-1, Rokkodia, Nada-Ku, Kobe, 657-8501 Japan. E-mail: kojima@cs.kobe-u.ac.jp

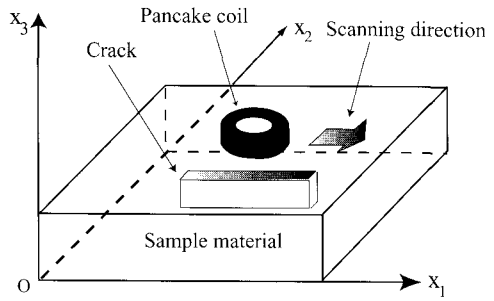

Fig. 1 : An illustration of inspection process

Some previous efforts have focused on QNDE based on the measurements of thermal diffusivity (See Banks and Kojima, 1989 and Banks et al, 1990). In this paper, the similar method is applied to the magnetic inverse problem arising in eddy current inspection. The crack shape is characterized by the unknown function on the boundary and the nonlinear output least square problem is considered for estimating the unknown function. To solve the nonlinear optimization problem, there are several ways of evaluating the gradient of the output least square error with respect to the unknown function. In this approach, the discrete analogue of the continuous shape design method is used with the background knowledge of material derivative. This method is a natural extension of the calculus of variation associated with the system design (See Pironneau, 1983 for more details).

This paper is organized as follows. In Section 2, the mathematical modeling of the inspection process is discussed. Measuring impedance trajectory by the pancake coil is derived from the Maxwell's equations and the Biot-Savart's law. In Section 3, a parameter estimation technique is proposed for estimating the shape of surface crack on the plate. The crack is characterized by the finite number of unknown coefficients based on B-spline approximations. The estimation scheme is proposed using the hybrid scheme of the finite element and the boundary element method. In Section 4, a computational method is given for evaluating the gradient of the output least square error with respect to the unknown parameters. Final part of this paper is devoted to results of computational experiments in order to demonstrate the efficacy of the proposed computational method.

2. Mathmatical Model of Inspection

The ECT analysis is described by the magnetic vector potential $\mathbf{A}$ and the electric scalar potential ϕ in three dimensions. Let (t, x) be the time t $(0 \leq t < \infty)$ and the location $x = (x_1, x_2, x_3)$ in R^3. Let V be a bounded domain of the sample in R^3 and S be its boundary corresponding to material inspected. Our attention is focused on a isotropic homogeneous plate as shown in Fig. 1. The mechanism of ECT is described in the following way. First, the force current density vector is applied to the pancake type probe coil in Fig. 1. Then the corresponding eddy current is generated inside the conductor near the coil. Then the impedance of the coil is affected due to the existence of the eddy current. The eddy current testing is to detect and characterize the crack inside the conductor by analyzing the coil impedance change due to the eddy current. As is well-known, the mathematical model of eddy current testing can be derived by Maxwell's equations, i. e.,

$$\nabla \cdot \mathbf{E} = 0 \tag{1}$$

$$\nabla \cdot \mathbf{B} = 0 \tag{2}$$

$$\nabla \times \mathbf{E} = -\frac{\partial \mathbf{B}}{\partial t} \tag{3}$$

$$\nabla \times \mathbf{H} = \mathbf{J} \tag{4}$$

where $\mathbf{E}, \mathbf{B}, \mathbf{H}$, and $\mathbf{J}$ are the electric field intensity, the magnetic flux density, the magnetic field intensity, and the current density vector, respectively. The solutions of the partial differential equations (1) through (4) are only obtained when additional constraints are imposed. In ECT, the constitutive laws also hold:

$$\mathbf{J} = \mathbf{J}_s + \sigma \mathbf{E} \tag{5}$$

$$\mathbf{B} = \mu \mathbf{H} \tag{6}$$

where $\mathbf{J}_s$, σ, and μ denote the applied source current of the coil probe, the electrical conductivity, and the magnetic permeability, respectively.. In general, the eddy current model is formulated by the electrical scalar potential ϕ and the magnetic vector potential $\mathbf{A}$ instead of $\mathbf{E}$ and $\mathbf{B}$. Those potential formulations are particularly convenient when the electromagnetic problem is driven by a well-defined source current distribution. More precisely, the model can

be formulated by

$$\mathbf{E} = -\frac{\partial}{\partial t}(\mathbf{A} + \nabla\Phi) \quad (7)$$

$$\mathbf{B} = \nabla \times \mathbf{A} \quad (8)$$

where Φ denotes the time integration of the electric scalar potential ϕ defined by

$$\Phi(t) = \int_{-\infty}^{t} \phi(\tau)\, d\tau. \quad (9)$$

For convenience of discussions, the domain is divided into the air region and the conductor region. Then the governing equation in air region $(R^3 - V)$is then expressed by

$$-\frac{1}{\mu_0}\nabla^2\mathbf{A} = \mathbf{J}_s \quad \text{in } R^3 - V. \quad (10)$$

where μ_0 denotes the magnetic permeability in air. Since the boundary of the system eqn.(10) becomes semi-infinite, the above equation can be represented by a boundary integral equation. The fundamental solution of eqn.(10) has the representation

$$u^*(x, x') = (4\pi|x - x'|)^{-1}. \quad (11)$$

Then, from the system eqn.(10), the solution on the boundary of the conductor satisfies the following boundary integral equation,

$$\frac{1}{2}\mathbf{A}(x_i) + \int_S \frac{\partial u^*(x_i, x')}{\partial n}\mathbf{A}(x')d\Gamma(x') - \int_S u^*(x_i, x')\frac{\partial \mathbf{A}}{\partial n}(x')d\Gamma(x') = \mu_0 \int_{V_c} u^*(x_i, x')\mathbf{J}_s(x')dx' \quad \text{for } x_i \in S \quad (12)$$

where $d\Gamma$ denotes the boundary measure and V_c denotes the region of the pancake coil. The eddy current in the conductor region is governed by

$$-\frac{1}{\mu_0}\nabla^2\mathbf{A} + \sigma\left(\frac{\partial \mathbf{A}}{\partial t} + \nabla\phi\right) = 0 \quad (13)$$

$$\nabla \cdot \sigma\left(\frac{\partial \mathbf{A}}{\partial t} + \nabla\phi\right) = 0 \text{ in } V \quad (14)$$

where μ_0 denotes the magnetic permeability of the air. It is noted that the magnetic permeability of SG tube is equal to that of air since INCONEL600 used for SG tube is non magnetic material. Since the alternative current source is applied in real eddy current testing, it is convenient to use the complex phasor representation. Suppose that the alternative current source is given by

$$\mathbf{J}_s = \bar{\mathbf{J}}_s \cos(\omega t) \quad (15)$$

where $\omega = 2\pi f$ is the angular frequency corresponding to the applied frequency f. Then the eddy current model considered here is represented by

$$\frac{1}{\mu_0}\nabla^2\mathbf{A} = j\omega\sigma(\mathbf{A} + \nabla\Phi) \quad (16)$$

$$j\omega\nabla \cdot \sigma(\mathbf{A} + \nabla\Phi) = 0 \quad \text{in} \quad V, \quad (17)$$

with the interface matching condition eqn.(12) at S. Thus the eddy current density in conductor can be evaluated as

$$\mathbf{J}_e = -j\omega\sigma(\mathbf{A} + \nabla\Phi). \quad (18)$$

The measurements can be made by the impedance change caused by the eddy current in the conducting sample. By virtue of the Biot-Savart's law, the magnetic vector potential of the coil caused by the eddy current is obtained by

$$\mathbf{A}_e(x) = \mu_0 \int_V u^*(x, x')\mathbf{J}_e(x')\, dx' \quad \text{for } x \in V_c. \quad (19)$$

Thus the impedance change due to the eddy current can be computed as

$$\Delta Z = \Delta R + j\omega\Delta L = -j\omega N \oint \mathbf{A}_e\, dl/I, \quad (20)$$

where $\Delta R, \omega\Delta L, N$ and I denote the resistivity of the impedance change, the reactance change, the number of coil turns, and coil current per turn, respectively. Consequently, the relation between the input and the output is described by the following map:

$$\mathbf{J}_s \longrightarrow \Delta Z \quad (21)$$

through eqns. (12) and (15) through (20).

3. Nondestructive Evaluation by Parameter Estimation

The inverse problem considered here is to estimate a crack shape by measuring the impedance trajectory ΔZ in pancake type coil. To this end,

the admissible paramcter class is given by approximating a crack shape. By approximating the mapping of $\mathbf{J}_s$ into ΔZ in a finite dimensional space, the parameter-to-data mapping can be constructed. Then the domain identification problem is converted into a parameter estimation problem. The remaining part of this section is devoted to a computational method for solving the parameter estimation problem.

3.1. Admissible Parameter Class:

The dimension of a test piece is preassigned as $l_1 \times l_2 \times l_3$. Let c_l and c_w be the length and the width of a crack. For the convenience of discussions, the crack is located at the center of the test piece,

$$C_r = (\frac{l_1 - c_l}{2}, \frac{l_1 + c_l}{2}) \times (\frac{l_2 - c_w}{2}, \frac{l_2 + c_w}{2}). \quad (22)$$

To characterize the shape of the surface crack, the curved function on (x_1, x_2) is defined by

$$\begin{aligned} x_3 &= h(x_1, x_2; \mathbf{q}) \\ &= \begin{cases} \sum_{i=1}^{M} q_i^M B_i^M(x_1) \text{ for } (x_1, x_2) \in C_r \\ l_3 \text{ (inner crack)} \\ 0 \text{ (outer crack)} \\ \quad \text{for } (x_1, x_2) \in (0, l_1) \times (0, l_2) - C_r \end{cases} \end{aligned} \quad (23)$$

Taking into account that the width of the crack is very narrow, the depth of the crack is characterized by a simple B-spline function (See e.g., de Boor (1978)) where $\{B_i^M\}_{i=1}^M$ are a sequence of B-spline functions with knot sequence such that

$$\Delta_M = \left\{ \{x_1^i\}_{i=1}^M \;\middle|\; \frac{l_1 - c_l}{2} = x_1^1 \le x_1^2 \le \cdots \le x_1^M = \frac{l_1 + c_l}{2} \right\}. \quad (24)$$

The Fourier coefficient vector $\mathbf{q} = \{q_i^M\}_{i=1}^M$ denotes a constant parameter vector to be identified among values in a given admissible parameter set Q_{ad},

$$Q_{ad} = \{\mathbf{q} \in R^M \mid 0 < \overline{q}_L \le q_i \le \overline{q}_U < l_3 (i = 1, \cdots, M)\}, \quad (25)$$

where $\overline{q}_L$ and $\overline{q}_U$ are given constants in R^M. Figure 2 illustrates dimensions of a sample specimen with a inner crack. It is noted that the location, the size of crack, and the orientation of the crack are preliminary determined by measurement data.

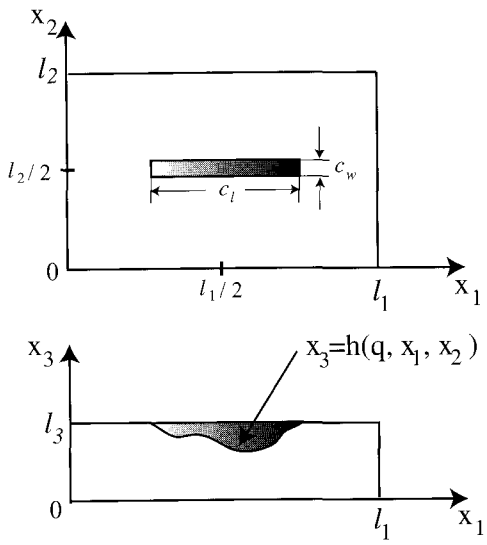

Fig. 2 : Dimension of a sample specimen with defect

3.2. Approximate Model with the Unknown Parameters :

The precise numerical method for solving the input-output mapping defined by eqn.(21) plays an essential role in formulating the identification problem treated here. Although the finite element method using the nodal elements is a simple scheme and is easy to build up the computer program, it is required to remesh finite elements at each location of pancake probe coil. This remeshing procedures cause the considerable amount of computational volume for the problem considered here. Since there is no need to remesh the finite element decomposition, the boundary element method has an advantage for the problem considered here but the serious computational efforts are necessary for implementing numerical integration of boundary element matrices. In this paper, taking into account that the system equation can be defined on the closed domain (conductor region V) and on the open domain (air region $R^3 - \overline{V}$), the hybrid scheme of the finite element and the boundary element method is applied to this problem. More precisely, the finite element method is adopted in the conductor region V, while the boundary element method is used in the air $R^3 - V$ including the coil region. The practical implementation of numerical technique is owed to Matsuoka

(1987). The nodes of finite elements are given by the coordinates that depend on the unknown parameter vector $\mathbf{q} = \{q_i\}_{i=1}^{M}$. From eqn.(22), the crack region is defined on

$$V_r(\mathbf{q}) = \begin{cases} \bar{C}_r \times [h(\mathbf{q}; x_1, x_2),\ l_3] \\ \qquad \text{for the outer crack} \\ \bar{C}_r \times [0,\ h(\mathbf{q}; x_1, x_2)] \\ \qquad \text{for the inner crack} \end{cases} \tag{26}$$

where $\bar{C}_r$ implies the closure set of C_r and $[\cdot, \cdot]$ denotes the closed interval on x_3-axis. Thus the domain of the conductor with the unknown crack is defined by

$$V_c(\mathbf{q}) = V_0 - V_r(\mathbf{q}) \tag{27}$$

where V_0 means the 'perfect' sample material without crack, i.e.,

$$V_0 = \left\{ \ x = (x_1, x_2, x_3) \ \middle| \ 0 < x_i < \tilde{l}_i, \quad (i = 1, 2, 3) \ \right\}.$$

The corresponding boundary with the surface crack is given by $S_c(\mathbf{q})$. Let us choose $\cup_{N_h=1}^{\infty} \{\psi_i^{N_h}\}_{i=1}^{N_h}$ as a set of basis functions in $H^1(V(\mathbf{q}))$. The approximation subspaces can be chosen as:

$$H^{N_h} = \mathrm{span}\{\psi_1^{N_h}, \psi_2^{N_h}, \cdots, \psi_{N_h}^{N_h}\}. \tag{28}$$

Then the magnetic potential and time integration of the electric scalar potential are approximated by

$$A \approx \sum_{i=1}^{N_h} \{A_{1i}^e, A_{2i}^e, A_{3i}^e\} \psi_i^{N_h},$$
$$\Phi \approx \sum_{i=1}^{N_h} \Phi_i^e \psi_i^{N_h}.$$

Let

$$\{\mathbf{A}_d\} = \{A_1^e, A_2^e, A_3^e\}^T, \qquad \{\Phi_d\} = \{\Phi^e\}^T$$

be the coefficient vector of A and Φ, respectively. Then the hybrid FEM-BEM scheme for eqns. (16) and (17) with eqn.(12) is represented by

$$[L + K](\mathbf{q}) \begin{Bmatrix} A_d \\ \Phi_d \end{Bmatrix} = \{F\}(\mathbf{q}; J_o), \tag{29}$$

(See Matsuoka (1987) for more details). In eqn.(29), L is the element matrix given by

$$[L] = \begin{bmatrix} [L_1] & 0 & 0 & [L_{21}] \\ 0 & [L_1] & 0 & [L_{22}] \\ 0 & 0 & [L_1] & [L_{23}] \\ [L_{21}]^T & [L_{22}]^T & [L_{23}]^T & [L_3] \end{bmatrix}, \tag{30}$$

where the $(k, l) \in \{1, \cdots, N_h\}$ component of each block matrix is denoted by

$$[L_1]_{kl} = \int_{V(\mathbf{q})} \left\{ \frac{1}{\mu_0} (\nabla \psi_k^{N_h}) \cdot (\nabla \psi_l^{N_h}) + \sigma j\omega \psi_k^{N_h} \psi_l^{N_h} \right\} dx \tag{31}$$

$$[L_{2m}]_{kl} = \sigma j\omega \int_{V(\mathbf{q})} \psi_k^{N_h} \frac{\partial \psi_l^{N_h}}{\partial x_m}\, dx \quad \text{for } m = 1, 2, 3, \tag{32}$$

and

$$[L_3] = \mu_0 \sigma j\omega [L_1], \tag{33}$$

respectively. Denoting the source point by x_i and from eqn.(11), the boundary element vectors $\{U^*\}$ and $\{\partial U^*/\partial n\}$ are defined by

$$\{U^*\}_k = u^*(x_k, x), \tag{34}$$

$$\left\{ \frac{\partial U^*}{\partial n} \right\}_k = \frac{\partial u^*}{\partial n}(x_k, x) \quad \text{for } x, x_k \in S_c(\mathbf{q}), \tag{35}$$

respectively. The element matrix K in eqn.(29) is then given by

$$[K] = \begin{bmatrix} [K_0] & 0 & 0 \\ 0 & [K_0] & 0 \\ 0 & 0 & [K_0] \end{bmatrix}, \tag{36}$$

where

$$[K_0] = \frac{1}{2} \left\{ [M][G]^{-1}[H] + ([M][G]^{-1}[H])^T \right\}.$$

The (k, l)-component of the matrix M is represented by

$$[M]_{kl} = \frac{1}{\mu_0} \int_{S_c(\mathbf{q})} [\psi_k^{N_h}\big|_{S_c(\mathbf{q})}][\psi_l^{N_h}\big|_{S_c(\mathbf{q})}]\, d\Gamma, \tag{37}$$

and the matrices $[G]$ and $[H]$ are a single layer and double layer potentials given by

$$[G]_{kl} = \frac{1}{\mu_0} \int_{S_c(\mathbf{q})} \{U^*(\mathbf{q})\}_k \left[\frac{\partial \psi_l^{N_h}}{\partial n}\bigg|_{S_c(\mathbf{q})} \right] d\Gamma, \tag{38}$$

$$[H]_{kl}=\frac{1}{\mu_0}\int_{S_c(\mathbf{q})}\left\{\frac{\partial U^*}{\partial n}(\mathbf{q})\right\}_k\left[\psi_l^{N_h}\Big|_{S_c(\mathbf{q})}\right]d\Gamma, \quad (39)$$

respectively. The element vector of eqn.(29) is given by

$$\{F\}=[[M][G]^{-1}\{F_1\},[M][G]^{-1}\{F_2\},[M][G]^{-1}\{F_3\}]^T,$$

$$\{F_n\}_k = \int_{V^c}\{U_c^*(\mathbf{q})\}_k J_o^n\, dx \quad \text{for } n=1,2,3,$$

where $\{U_c^*\}$ is given by

$$\{U_c^*\}_k = u^*(x_k,x) \quad \text{for } x\in V^c, x_k\in S(\mathbf{q}). \quad (40)$$

Thus the model output of impedance trajectory is represented by

$$\Delta Z_d(\mathbf{q},J_d)=\{C\}(\mathbf{q})^T\left\{\begin{array}{c}A_d\\ \Phi_d\end{array}\right\} \quad (41)$$

where $\{C\}$ is the interpolation vector corresponding to the model output eqn.(20) given by

$$\{C\}=\{C_1,C_1,C_1,C_2\} \quad (42)$$

where the k-th ($k\in\{1,\cdots,N_h\}$) component of each block vector is given by

$$\{C_1\}_k=-\sigma\mu_0\omega^2 N\oint\left\{\int_{V_c(\mathbf{q})}U_c^*(\mathbf{q})\psi_k^{N_h}dx\right\}dl, \quad (43)$$

$$\{C_2\}_k=-\sigma\mu_0\omega^2 N\oint\left\{\int_{V_c(\mathbf{q})}U_c^*(\mathbf{q})\mathrm{div}\psi_k^{N_h}dx\right\}dl. \quad (44)$$

Consequently, the parameter-to-output mapping

$$(\mathbf{q},\mathbf{J}_s)\longrightarrow\Delta Z_d(\mathbf{q},\mathbf{J}_s) \quad (45)$$

is obtained by solving eqns. (29) and (41).

3.3. Parameter Estimation Problem :

The parameter estimation problem is formulated as follows:

Given an appropriate frequency ω and a set of current forces $\{\mathbf{J}_s^i\}_{i=1}^{N_p}$ in accordance with the coil movement, and measure the corresponding impedance trajectory $Y_d=\{Y_d^i\}_{i=1}^{N_p}$, find the optimal $\mathbf{q}=\mathbf{q}^*$ which minimizes the output least square error

$$E(\mathbf{q})=\frac{1}{2}\sum_{i=1}^{N_p}\left|\Delta Z_d(\mathbf{q},\mathbf{J}_s^i)-Y_d^i\right|^2 \quad (46)$$

with respect to $\mathbf{q}\in Q_{ad}$ subject to eqns. (29) and (41).

To solve the above parameter estimation problem, so many discrete optimization routines are applicable (See Kojima, 1996). For the numerical results reported in this paper, the trust region algorithm with linear inequality constraints (Carter, 1987) were implemented. The advantage of this algorithm is its global convergence properties; namely, this algorithm make it possible to obtain convergence to a critical point (optimal solution), even from starting points (initial guess) that are far away from the optimal solution.

Estimation Algorithm: Let $\hat{\mathbf{q}}^{(0)}$ be the initial guess and the trust region $\Delta^{(0)}$ be given. Set the parameter $\mu\in(0,1)$. For $k=1,2,\cdots$, iterate the following step:

Step 1: Compute $E(\hat{\mathbf{q}}^{(k)})$ and the model $\phi(\hat{\mathbf{q}}^{(k)})$ defined by

$$\begin{aligned}\phi^{(k)}(\mathbf{q}) &= E(\hat{\mathbf{q}}^{(k)})+<\{\mathbf{g}(\hat{\mathbf{q}}^{(k)})\},\{\delta\mathbf{q}\}>\\ &\quad+\frac{1}{2}<\{\delta\mathbf{q}\},[\mathbf{B}(\hat{\mathbf{q}}^{(k)})]\{\delta\mathbf{q}\}> \end{aligned}\quad (47)$$

where $\delta\mathbf{q}=\mathbf{q}-\hat{\mathbf{q}}^{(k)}$ and where $\{\mathbf{g}\}$ and $[\mathbf{B}]$ denote the gradient and the approximated Hessian of the cost eqn. (46).

Step 2: Determine an approximate solution $\delta\mathbf{q}=\mathbf{s}_k$ to subproblem

$$\min\left\{\phi^{(k)}(\hat{\mathbf{q}}^{(k)}+\delta\mathbf{q}) \quad | \quad |\delta\mathbf{q}|\le\Delta^{(k)}\right\} \quad (48)$$

Step 3: Compute

$$\rho^{(k)}=\frac{E(\hat{\mathbf{q}}^{(k)}+\mathbf{s}_k)-E(\hat{\mathbf{q}}^{(k)})}{\phi(\mathbf{s}_k)} \quad (49)$$

Step 4: If $\rho^{(k)}>\mu$ then $\hat{\mathbf{q}}^{(k+1)}=\hat{\mathbf{q}}^{(k)}+\mathbf{s}_k$. Otherwise $\hat{\mathbf{q}}^{(k+1)}=\hat{\mathbf{q}}^{(k)}$.

Step 5: Update the model $\phi^{(k)}$ and the trust region $\Delta^{(k)}$ in the appropriate manner.

The gradient of the cost eqn. (47) with respect to the unknown parameter $\mathbf{q}$ can be evaluated by the discrete analogue of the material derivative. Using the co-state approach, the gradient of the cost can be computed as follows:

$$\{\mathbf{g}(\mathbf{q})\}_m = \frac{\partial E}{\partial q_m}(\mathbf{q})$$
$$= \sum_{i=1}^{N_p} \frac{\partial \Delta Z_d(\mathbf{q}, \mathbf{J}_s^i)}{\partial q_m}(Z_d(\mathbf{q}, \mathbf{J}_s^i) - Y_d^i)$$
$$= \sum_{i=1}^{N_p} \left\{ \left\langle \left\{ \frac{\partial C}{\partial q_m}(\mathbf{q}) \right\} (Z_d(\mathbf{q}, \mathbf{J}_s^i) - Y_d^i), \begin{Bmatrix} A_d \\ \Phi_d \end{Bmatrix} (\mathbf{q}, \mathbf{J}_s^i) \right\rangle \right.$$
$$\left. + \left\langle \left[\frac{\partial L}{\partial q_m} + \frac{\partial K}{\partial q_m} \right] \begin{Bmatrix} A_d \\ \Phi_d \end{Bmatrix} (\mathbf{q}, \mathbf{J}_s^i) - \left\{ \frac{\partial F}{\partial q_m} \right\} (\mathbf{q}, J_s^i), \begin{Bmatrix} A_d^* \\ \Phi_d^* \end{Bmatrix} (\mathbf{q}, \mathbf{J}_s^i) \right\rangle \right\} \quad (m = 1, 2, \cdots, M), \quad (50)$$

where $\{A_d^*, \Phi_d^*\}^T$ is the solution of the adjoint system eqn. (29):

$$[L+K]^T(\mathbf{q}) \begin{Bmatrix} A_d^* \\ \Phi_d^* \end{Bmatrix} = -\{C\}(\mathbf{q}) \left(\{C\}(\mathbf{q})^T \begin{Bmatrix} A_d \\ \Phi_d \end{Bmatrix} - Y_d^i \right). \quad (51)$$

4. Computation of the Gradient

There are several ways of evaluating the gradient of the cost with respect to the boundary shape. By change of the variables which bring the variable domains into a fixed domain the gradient of the cost can be computed using the sensitivity equation with the unknown coefficients. This method was successfully used in the inversions of the thermal tomography (Banks and Kojima, 1989, Banks et al, 1990). However there exist inherent limitations for the applicability to QNDE due to the complexity of practical geometrical constraints, such as the shape of the crack. Therefore, in this paper, the material derivative is adopted for evaluating the unknown shape of crack (See Pironneau, 1983). More precisely, the gradient of the cost eqn. (47) can be evaluated by perturbing the nodes at the surface crack boundary and by moving the associated interior nodes. For the economy of computational volumes, the conductor domain $V(\mathbf{q})$ is decomposed into two sub-domains, i. e.,

$$V_c(\mathbf{q}) = V_s(\mathbf{q}) \bigcup V_o \quad (52)$$

where $V_s(\mathbf{q})$ denotes the region of the interest associated with the neighborhood of the surface crack. The region of the interest in the identification problem is selected as

$$V_s(\mathbf{q}) = \{x = (x_1, x_2, x_3) \,|\, \overline{x}_i^L < x_i < \overline{x}_i^U, (i = 1, 2),$$

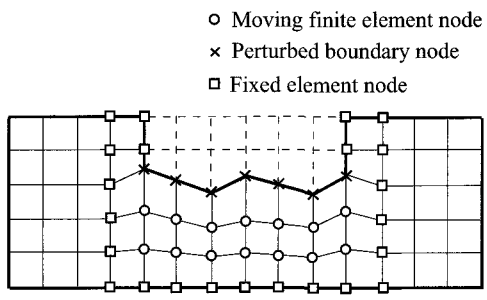

Fig. 3 Sectional plan of the finite element decomposition in the region of interest

$$h(\mathbf{q}; x_1, x_2) < x_3 < l_3 \text{ for the outer crack},$$
$$0 < x_3 < h(\mathbf{q}; x_1, x_2) \text{ for the inner crack}\} \quad (53)$$

In $V_s(\mathbf{q})$, $\overline{x}_i^L$ and $\overline{x}_i^U$ must be chosen as

$$0 < \overline{x}_1^L < \frac{l_1 - c_l}{2}, \quad \frac{l_1 + c_l}{2} < \overline{x}_1^U < l_1 \quad (54)$$
$$0 < \overline{x}_2^L < \frac{l_2 - c_w}{2}, \quad \frac{l_2 + c_w}{2} < \overline{x}_2^U < l_2. \quad (55)$$

Let $\mathbf{X} = \{\mathbf{x}_i^h = (x_1^i, x_2^i, x_3^i)\}_{i=1}^{N_h}$ be the set of the coordinates of the nodes in the conductor and those are assumed to be constructed as

$$\mathbf{X}_s = \{\mathbf{x}_i^h\}_{i=1}^{N_s} \in V_s(\mathbf{q}), \ \mathbf{X}_o = \{\mathbf{x}_i^h\}_{i=N_s+1}^{N_h} \in V_o. \quad (56)$$

Furthermore, the set of the nodes in the region of the interest is divided into three parts:

$$\mathbf{X}_s(\mathbf{q}) = \mathbf{X}_f \bigcup \mathbf{X}_r(\mathbf{q}) \bigcup \mathbf{X}_a(\mathbf{q}), \quad (57)$$

where $\mathbf{X}_f$ denotes the set of the fixed nodes, $\mathbf{X}_r$ denotes the set of the nodes at the surface crack of the boundary, and $\mathbf{X}_a$ is the set of the moving nodes associated with the set $\mathbf{X}_r$. Figure 3 illustrates the

sectional plan of the finite element decomposition in the region of interest. As depicted in Fig.3, the coordinates of nodes in $\mathbf{X}_r(\mathbf{q})$ are determined by

$$\mathbf{x}_i^h(\mathbf{q}) = (\ x_1^i,\ x_2^i,\ h(\mathbf{q}, x_1^i, x_2^i)\ ) \in \mathbf{X}_r(\mathbf{q}). \quad (58)$$

The coordinates of $\mathbf{X}_a$ can be determined by the fixed nodes $\mathbf{X}_f$ and $\mathbf{X}_a$. Namely, all nodes of $\mathbf{X}_a$ are constructed from

$$\mathbf{x}_i^h(\mathbf{q}) = (\ x_1^i,\ x_2^i,\ \Phi_i(\mathbf{q}; h)\ ) \in \mathbf{X}_a, \quad (59)$$

where Φ_i denotes the continuous mappings of the depth function $h(\mathbf{q})$ to x_3^i. For instance, the mapping Φ_i for the inner crack case is given by

$$\Phi_{m(i)}=\begin{cases} m(i) \times h(\mathbf{q}, x_1, x_2)/N_s \text{ (inner crack)} \\ h+(l_3-h(\mathbf{q}, x_1, x_2))/N_s \text{ (outer crack)} \end{cases} \quad (60)$$

$$(m(i) = 1, \cdots, N_s\ ;\ i = 1, 2, \cdots, M).$$

The finite element decomposition of $V_r(\mathbf{q})$ can be determined by the coordinate systems $\mathbf{X}_r$. Let $\{e_i\}_{i=1}^{K_r}$ and $\{e_i^b\}_{i=1}^{K_r^b}$ be the finite elements covering $V_r(\mathbf{q})$ and the related boundary $S_r(\mathbf{q})$. It is noted that the set of finite elements $\{e_i(\mathbf{q})\}_{i=1}^{K_r}$ and the set of boundary elements $\{e_i^b(\mathbf{q})\}_{i=1}^{K_r^b}$ are determined from eqns. (58) and (59). To compute eqn. (50), the sequence of the mappings $\{T_i(\mathbf{q})\}_{i=1}^{K_r}$ of each finite element to a reference element such that

$$e_i(\mathbf{q}) = T_i(\mathbf{q}) \circ \tilde{e} \quad \text{for } i = 1, \cdots, K_r \quad (61)$$

as depicted in Fig. 4. Similarly, the set of mappings $\{T_i^b(\mathbf{q})\}_{i=1}^{K_r^b}$ can be constructed as:

$$e_i^b(\mathbf{q}) = T_i^b(\mathbf{q}) \circ \tilde{e}^b \quad \text{for } i = 1, \cdots, K_r^b \quad (62)$$

as depicted in Fig. 4. Then the partial derivative of the matrix $[L]$ can be evaluated as

$$\left[\frac{\partial L}{\partial q_m}(\mathbf{q})\right] = \begin{bmatrix} [\partial L_1/\partial q_m] & 0 & 0 & [\partial L_{21}/\partial q_m] \\ 0 & [\partial L_1/\partial q_m] & 0 & [\partial L_{22}/\partial q_m] \\ 0 & 0 & [\partial L_1/\partial q_m] & [\partial L_{23}/\partial q_m] \\ [\partial L_{21}/\partial q_m]^T & [\partial L_{22}/\partial q_m]^T & [\partial L_{23}/\partial q_m]^T & \mu_0 \sigma j\omega [\partial L_1/\partial q_m] \end{bmatrix} \quad \text{for } m = 1, 2, \cdots, M, \quad (63)$$

where

$$\left[\frac{\partial L_1}{\partial q_m}\right]_{kl} = \int_{\tilde{e}} \sum_{i=1}^{K_s} \frac{\partial}{\partial q_m} \left[\left\{ \frac{1}{\mu_0} \tilde{\nabla} \tilde{\psi}_k^{N_h} \cdot (\tilde{\nabla} T_i(\mathbf{q}))^{-T} (\tilde{\nabla} T_i(\mathbf{q}))^{-1} (\tilde{\nabla} \tilde{\psi}_l^{N_h}) + \sigma j\omega \tilde{\psi}_k^{N_h} \tilde{\psi}_l^{N_h} \right\} \left| \det \tilde{\nabla} T_i(\mathbf{q}) \right| \right] d\tilde{x}, \quad (64)$$

$$\left[\frac{\partial L_{2n}}{\partial q_m}\right]_{kl} = \sigma j\omega \int_{\tilde{e}} \sum_{i=1}^{K_s} \frac{\partial}{\partial q_m} \left[\tilde{\psi}_k^{N_h} \left\{ (\tilde{\nabla} T_i(\mathbf{q}))^{-1} \tilde{\nabla} \tilde{\psi}_l^{N_h}) \right\}_n \left| \det \tilde{\nabla} T_i(\mathbf{q}) \right| \right] d\tilde{x} \quad \text{for } n = 1, 2, 3. \quad (65)$$

In order to evaluate the sensitivity of the matrix $[K](\mathbf{q})$, the partial derivative of the matrices $[M](\mathbf{q})$, $[G](\mathbf{q})$, and $[H](\mathbf{q})$ are given by

$$\left[\frac{\partial M}{\partial q_m}\right]_{kl} = \frac{1}{\mu_0} \int_{\tilde{e}^b} \left(\tilde{\psi}_k^{N_h} \Big|_{\tilde{e}^b} \tilde{\psi}_l^{N_h} \Big|_{\tilde{e}^b} \right) \sum_{i=1}^{K_s^b} \frac{\partial}{\partial q_m} \left[\left| \det \tilde{\nabla} T_i^b(\mathbf{q}) \right| \right] d\tilde{\Gamma}, \quad (66)$$

$$\left[\frac{\partial G}{\partial q_m}\right]_{kl} = \frac{1}{\mu_0} \int_{\tilde{e}^b} \sum_{i=1}^{K_s^b} \frac{\partial}{\partial q_m} \left[\{\tilde{U}_i^*(\mathbf{q})\}_k \left\{ (\tilde{\nabla} T_i^b(\mathbf{q}))^{-1} \tilde{\nabla} \tilde{\psi}_l^{N_h} \cdot \mathbf{n}(\mathbf{q}) \right\} \Big|_{\tilde{e}^b} \left| \det \tilde{\nabla} T_i^b(\mathbf{q}) \right| \right] d\tilde{\Gamma}, \quad (67)$$

$$\left[\frac{\partial H}{\partial q_m}\right]_{kl} = \frac{1}{\mu_0} \int_{\tilde{e}^b} \sum_{i=1}^{K_s^b} \frac{\partial}{\partial q_m} \left[\left\{ (\tilde{\nabla} T_i^b(\mathbf{q}))^{-1} \{\tilde{\nabla} \tilde{U}_i^*(\mathbf{q})\}_k \cdot \mathbf{n}(\mathbf{q}) \right\} \tilde{\psi}_l^{N_h} \Big|_{\tilde{e}^b} \left| \det \tilde{\nabla} T_i^b(\mathbf{q}) \right| \right] d\tilde{\Gamma}. \quad (68)$$

Furthermore, the vectors $\{F_n\}(\mathbf{q})$, $\{C_1\}(\mathbf{q})$, and $\{C_2\}(\mathbf{q})$ are computed as

$$\left\{\frac{\partial F_n}{\partial q_m}\right\}_k = \int_{V^c} \frac{\partial}{\partial q_m} \left[\{U_c^*(\mathbf{q})\}_k\right] J_o^n \, d\tilde{x} \quad \text{for } n = 1, 2, 3, \tag{69}$$

$$\left\{\frac{\partial C_1}{\partial q_m}\right\}_k = -\sigma\mu_0\omega^2 N \oint \left(\int_{\tilde{e}^b} \sum_{i=1}^{K_c} \frac{\partial}{\partial q_m} \left[T_i(\mathbf{q})^{-1} \circ \tilde{U}_c^*(\mathbf{q}) \psi_k^{N_h} \left| \det \tilde{\nabla} T_i^b(\mathbf{q}) \right| \right] d\tilde{x} \right) dl, \tag{70}$$

$$\left\{\frac{\partial C_2}{\partial q_m}\right\}_k = -\sigma\mu_0\omega^2 N \oint \left\{ \int_{\tilde{e}^b} \sum_{i=1}^{K_c} \frac{\partial}{\partial q_m} \left[T_i(\mathbf{q})^{-1} \circ \tilde{U}_c^*(\mathbf{q}) \left(\tilde{\mathrm{div}} \psi_k^{N_h} \right) \left| \det \tilde{\nabla} T_i^b(\mathbf{q}) \right| \right] d\tilde{x} \right\} dl. \tag{71}$$

5. Computational Experiments

All experiments were carried out at Nuclear Engineering Ltd. in Osaka, Japan. First part of this section is devoted to the experimental set-up at the laboratory. Secondly, a forward analysis defined by eqn. (45) is tested for the purpose of the feasibility of the modeling of the inspection process. This is followed by a discussion in which the validity of the proposed algorithm using laboratory data is demonstrated.

5.1. Experimental Set-up :

Throughout experiments, a test piece is INCONEL600 which is used for the steam generator tubes of pressurized water type nuclear plants. The magnetic permeability μ_0 and the conductivity σ were taken as

$$\mu_0 = 4\pi \times 10^{-7} \text{ (H/m)} \quad \sigma = 1.0 \times 10^6 \text{ (S/m)}. \tag{72}$$

The size of the test piece was a square plate such that

$$l_1 = l_2 = 20, \quad l_3 = 1.25 \quad \text{(mm)}.$$

Test pieces which have different crack shapes were made using electric discharge machining (EDM crack). The width and the length of the EDM crack was

$$c_l = 10 \quad c_w = 0.2 \quad \text{(mm)}$$

and the crack was located in C_r given by eqn. (22). The several types of the EDM cracks which have different depth from 20 to 60% were used in the experiments. The coil has axisymmetric shape and is made of 140 turns. The height of the coil is 0.8 mm and its outer and inner diameters are 3.2 and 1.2 mm, respectively. Figure 5 depicts a pancake type probe coil manufactured in this experiment and the measurement set-up of experimental works. Figure 6 shows the schematic drawing of the experimental setup. A test sample is fixed on a $x_1 - x_2$ translation stage driven by servo-mechanism. The lift-off which means the distance between the test piece and the bottom of the pancake coil can be set by x_3 axial dial. A test piece on the $x_1 - x_2$ translation stage moves parallel to the x_1 direction, while the coil is fixed. The crack center is defined as $x_2 = 10$ mm. Impedance was measured from the center, $x_2 = 0$ mm till $x_2 = 10$ mm at every 1 mm. The lift-off was taken as 0.5 mm. The alternating current applied to the probe coil was set as 300 kHz. Alternating current is supplied by an impedance analyzer.

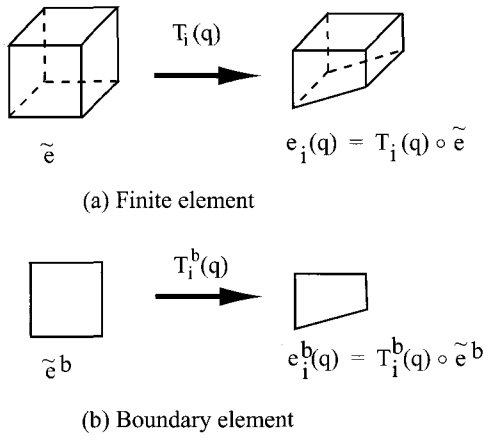

Fig. 4 Transformation mapping of finite and boundary elements

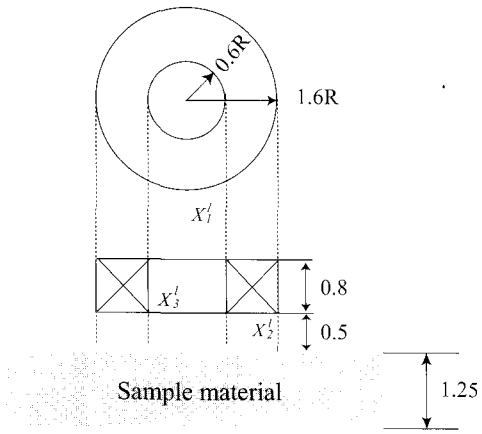

Fig. 5 Pancake type probe coil and measurement set-up in the experiments

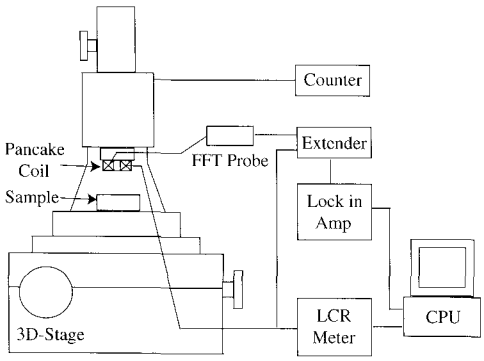

Fig. 6 : Schematic drawing of the experimental set-up

5.2. Forward Analysis for Parameter-to-Output Mapping :

The depth of EDM crack was approximated by eqn. (23). In the experiments, linear spline is adopted which implies the first order of B-splines. The dimensions of the unknown parameter vectors $\mathbf{q}$ were taken as $M = 6$. The corresponding numbers of knot sequences Δ_M in eqn. (24) were chosen as

$$\Delta_M = \{5.0, 7.0, 9.0, 11.0, 13.0, 15.0\}.$$

The test sample is divided into a finite number of brick elements $\{e_i\}_{i=1}^{K_h}$ and a number N_h of nodes defined by $\{\mathbf{x}_i = (x_1^i, x_2^i, x_3^i)\}_{i=1}^{N_h}$ are selected in $V(\mathbf{q})$. Each element is preassigned as an axiparallel rectangle with eight nodes at the vertices as shown in Fig. 7. The number of finite elements and nodes in the numerical experiments reported on here was

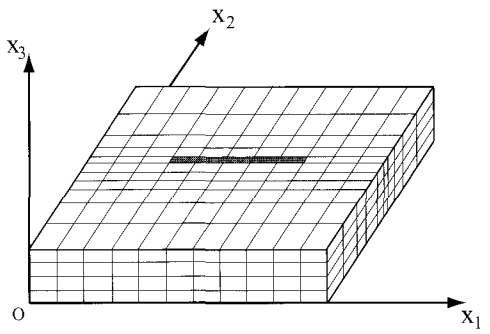

Fig. 7 Finite and boundary element decomposition of sample specimen in the experiments

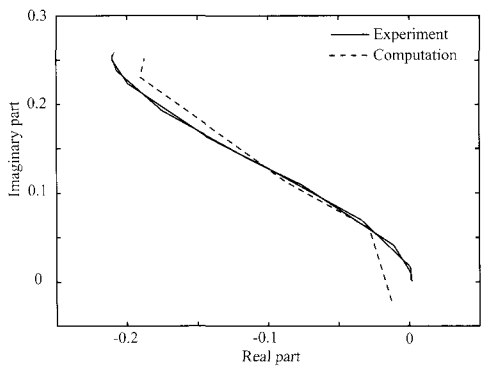

Fig. 8 ECT signals and simulated impedance trajectory for EDM crack with ID40% depth

set as $K_h = 474$ and $N_h = 720$, respectively. The corresponding boundary elements were taken from the surface of the finite elements of the test piece. Namely, each boundary element becomes axiparallel rectangle with four nodes at the vertices. In the experiments, the number of boundary elements and nodes were taken as $K_h^b = 442$ and $N_h^b = 444$, respectively. Figure 7 illustrates the finite and boundary element decomposition of the conductor.

The restriction of $\psi_i^{N_h}$ to any finite element e_i is given by a bilinear basis functions. To compute the impedance trajectory, the number of coil positions was set as $N_p = 9$ and those were located at

$$x_1^p = 0.002, x_2^p = 0.004, \cdots, x_9^p = 0.018.$$

Figures 8 and 9 represent the measurement data and the corresponding numerical solutions for the inner and outer defect with 40% depth, respectively.

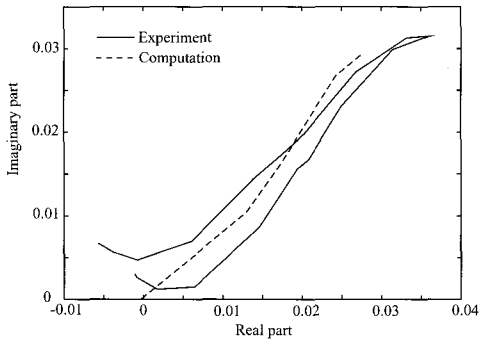

Fig. 9 ECT signals and simulated impedance trajectory for EDM crack with OD40% depth

Table 1 Category of crack shape in the experiments of inverse analyses

Experiments	Location of Crack	Shape of Depth
(1)	Outer Defect	Rectangular (60%)
(2)	Inner Defect	Rectangular (40%)
(3)	Outer Defect	Slope (60% – 20%)
(4)	Inner Defect	Slope (20% – 60%)

5.3. Inverse Analysis with Experimental Data :

In this subsection, results of using the proposed estimation procedures are reported. Test examples were performed for the crack shapes described in Table 1. Throughout numerical experiments, the value of the initial guesses were chosen as

$$\hat{\mathbf{q}}^{(0)} = \{0.625, 0.625, 0.625, 0.625, 0.625, 0.625\}$$

which implies the 50% depth (ratio to plate thickness) of the crack. For the implementation of the estimation algorithm given in Section 3, a Fortran software package "OPT2" (See Carter 1987) was used. The evaluation of the Hessian matrix $\mathbf{B}(\mathbf{q})$ is the computationally expensive parts of the proposed algorithm. Hence the Hessian was computed using the Broyden-Fletcher-Goldfarb-Shano (BFGS) secant update with safeguarding Hessian approximation (Also see Broyden for BFGS 1970 and see Carter 1987 for Hessian approximation). In each experiment, the optimization routine was implemented using rectangular trust regions. Table 2 reports the estimated parameter results and results of estimated

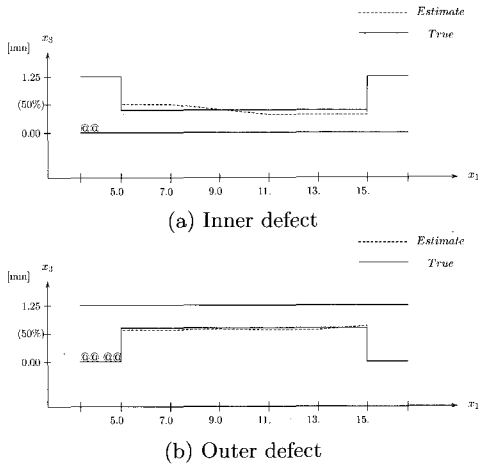

(a) Inner defect

(b) Outer defect

Fig. 10 True and estimated crack shape for EDM crack with 60% depth

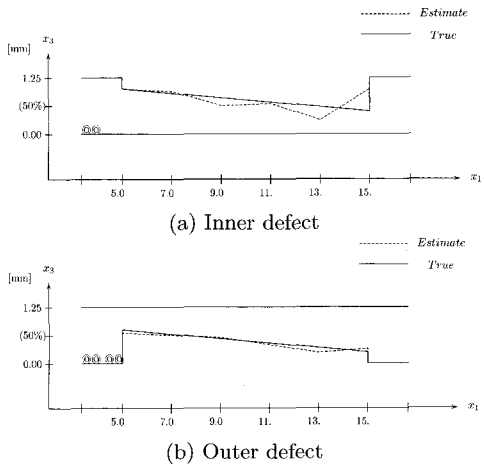

(a) Inner defect

(b) Outer defect

Fig. 11 True and estimated crack shape for EDM crack with 20 – 60% depth

shape and true shape are depicted in Figs. 10 and 11.

6. Concluding Remarks

A feasible computational method was proposed for detecting and characterizing crack in steam generator tubes of nuclear plants using the advanced ECT technique. The parameter estimation code was developed based on the hybrid use of FEM-BEM code that makes it possible to evaluate the probe impedance trajectory. To date, measurements for

Table 2 True and estimated values of the unknown parameters **q**

Defect Model		q_1 [mm]	q_2 [mm]	q_3 [mm]	q_4 [mm]	q_5 [mm]	q_6 [mm]	Accuracy $\left\lvert \frac{q^0}{q^*-q^0} \right\rvert$
(1) 60% OD	True	0.750	0.750	0.750	0.750	0.750	0.750	17.07
	Est.	0.703	0.703	0.725	0.703	0.703	0.795	
(2) 60% ID	True	0.500	0.500	0.500	0.500	0.500	0.500	45.45
	Est.	0.511	0.511	0.511	0.511	0.511	0.511	
(3) Slope OD	True	0.750	0.650	0.550	0.450	0.350	0.250	8.013
	Est.	0.676	0.627	0.574	0.415	0.238	0.326	
(4) Slope ID	True	1.000	0.900	0.800	0.700	0.600	0.500	4.162
	Est.	0.960	0.901	0.629	0.318	0.583	0.667	

the EDM cracks with $20-60\%$ depth and with $20-60\%$ slope were carried out and the estimation package was tested with these resulting data. The several results reported in Section 5 are representative of the findings obtained in these experiments. In all cases, the algorithm performed as well as or better than it did in the examples in Section 5. This fact provides rather conclusive evidence that structural flaws on the steam generator tubes can be successfully detected using the recent technology of the eddy current inspection. The current research includes both experimental and computational investigations to further refine the proposed method as well as to test other types of specimens (tube shape) and flaws (natural cracks) with regard to ease and accuracy in detection and characterization of cracks using the advanced ECT technique. The computational cost is the crucial part of the practical implementation of the proposed method. The of forthcoming intelligent analysis might reduce those costs. Exploration of this alternative is currently in progress.

Acknowlodgements

This study was supported in part by the Research Committee on Advanced Eddy Current Testing Technology of the Japan Society of Applied Electromagnetics and Mechanics through a grant from 5 PWR utilities and Nuclear Engineering Ltd. Thanks are extended to Messrs. Okamoto and Ohno who were my former students at Osaka Institute of Technology for their valuable computational works.

References

Banks, H.T. and Kojima, F. (1989) Boundary Shape Identification Problems in Two-dimensional Domains related to Thermal Testing of Materials, Quart. Appl. Math., Vol. 47, pp. 273-293

Banks, H.T., Kojima, F. and Winfree W.P. (1990) Boundary Estimation Problems arising in Thermal Tomography, Inverse Problems, Vol. 6, pp. 121-132

Bowler, J.R., Jenkins, S.A., Sabbagh, L.D., and Sabbagh, H.A. (1991) Eddy-current Probe Impedance due to a Volumetric Flaw, J. Appl. Phys., Vol. 70, No. 3, pp. 1107-1114

Bowler, J.R. (1995) Eddy Current Inversion using Gradient Method, *Studies in Applied Electromagnetics and Mechanics*, Vol. 8, IOS Press, Amsterdam, the Netherlands, pp. 31-40

Broyden, C.G. (1970) The Convergence of a Class of Double-Rank Minimization Algorithm, *J. Institute of Mathematics and Its Applications*, Vol. 6, pp. 76-90

Carter, R.G. (1987) Safeguarding Hessian Approximations in Trust Region Algorism, *Technical Report*, **TR87-12**, Department of Mathematical Sciences, Rice University

de Boor, C. (1978) *Practical Guide to Splines*, Springer, New York

Harrison, D.J., Jones L.D., and Burke S.K. (1996) Benchmark Problems for Defect Size and Shape Determination in Eddy-current Nondestructive Evaluation, J. Nondestructive Evaluation, Vol. 15, No. 1, pp. 21-34

Kojima, F. (1996) Computational Methods for Inverse Problems in Engineering Sciences. International Journal of Applied Electromagnetics and Mechanics, Vol. 7, pp. 1-16

Matsuoka, F (1987) Calculation of a Three Dimensional Eddy Current by the FEM-BEM Coupling Method, *Proc. IUTAM Conf. on Electromagnetomechanical Interactions in Deformable Solids and Structures*, North-Holland pp. 169-174

Pironneau, O (1983) *Optimal Shape Design for Elliptic Systems*, Springer, New York.

Sabbagh, H.A. and L.D. Sabbagh (1986) An Eddy-current Model for Three-dimensional Inversion, IEEE Trans. on Magnetics, Vol. MAG-22, No. 4, pp. 282-290

Takagi, T. et al. (1994) Benchmark Models of Eddy Current Testing for Steam Generator Tube: Experiment and Numerical Analysis, Int. J. Applied Electromagnetics in Materials, Vol. 5, pp. 149-162.

Takagi, T. et al. (1995) ECT research activities in JSAEM - Benchmark models of eddy current testing for steam generator tube (Part 1), *Studies in Applied Electromagnetics and Mechanics*, Vol. 8, IOS Press, Amsterdam, the Netherlands, pp. 253-264.

Takagi, T. et al. (1996). Electromagnetic NDE research activities in JSAEM, *Studies in Applied Electromagnetics and Mechanics*, Vol. 12, IOS Press, Amsterdam, the Netherlands, pp. 9-16.